Orbitally Forced Ice Sheet Fluctuations in Snowball Earth

Douglas I. Benn,[1,2*] Guillaume Le Hir,[3] Huiming Bao,[4] Yannick Donnadieu,[5] Christophe Dumas,[5] Edward J. Fleming,[1,6,7] Michael J. Hambrey,[8] Emily A. McMillan,[6] Michael S. Petronis,[9] Gilles Ramstein,[5] Carl T.E. Stevenson,[6] Peter M. Wynn,[10] Ian J. Fairchild[6]

---

[1]Department of Geology, The University Centre in Svalbard (UNIS), N-9171 Longyearbyen, Norway.

[2]School of Geography and Geosciences, University of St Andrews, St Andrews KY16 8YA, Scotland, UK.

[3]Institut de Physique du Globe de Paris, Paris, France

[4] Department of Geology and Geophysics, E235 Howe-Russell Complex, Louisiana State University, Baton Rouge, LA 70803, USA.

[5]Laboratoire des Sciences du Climat et de l'Environnement, CNRS-CEA, Gif-sur-Yvette, France

[6]School of Geography, Earth and Environmental Sciences, University of Birmingham B15 2TT, UK.

[7]Current address: CASP, West Building, 181A Huntingdon Road, Cambridge, CB3 0DH, UK

[8]Institute of Geography and Earth Sciences, Aberystwyth University, Aberystwyth, Wales, UK.

[9] Natural Resource Management, Environmental Geology,, New Mexico Highlands University, Las Vegas, New Mexico, USA.

[10]Lancaster Environment Centre, University of Lancaster, Lancaster LA1 4YQ, UK.

*Corresponding author. E-mail: Doug.Benn@unis.no

Snowball Earth theory provides a powerful framework for understanding Neoproterozoic panglaciations, although some predictions are apparently contradicted by geological evidence. Snowball theory posits that the panglaciations were terminated after millions of years of frigidity by a positive feedback, in which initial warming from rising atmospheric CO_2 was amplified by reduction of ice cover and planetary albedo (1, 2). This threshold behaviour implies that most of the glacial record was deposited in a brief 'melt-back' period (3), an interpretation apparently inconsistent with geological evidence for glacial-interglacial cycles in low palaeolatitudes (4-6). Here we use geological and geochemical evidence combined with numerical modeling experiments to reconcile these apparently conflicting views. New evidence from Svalbard (Norwegian High Arctic) indicates oscillating glacier extent and hydrological conditions within continental deposits of a Cryogenian glaciation, during a period when pCO_2 was uniformly high. Modeling experiments show that such oscillations can be explained by orbital forcing in the late stages of a 'Snowball' glaciation, while pCO_2 was rising towards the threshold required for complete melt-back. This enriched Snowball Earth theory can potentially explain complex successions observed at other localities.

The Wilsonbreen Formation in NE Svalbard contains a detailed record of environmental change during the Marinoan, the second of the major Cryogenian glaciations (650-635 Ma) (7, 8). At this time, Svalbard was located in the Tropics on the eastern side of Rodinia (9, 10). The <180 m thick Wilsonbreen Formation was deposited within a long-lived intracratonic sedimentary basin (11). It is subdivided into three members (W1, W2 and W3) based on the relative abundance of diamictite

and carbonate beds (7, 8; Fig. 1; Supplementary Figures 1 & 2). The occurrence throughout the succession of lacustrine sediments containing both precipitated carbonate and ice-rafted detritus, and intermittent evaporative carbonates and fluvial deposits, indicates that the basin remained isolated from the sea, consistent with eustatic sea level fall of several hundred metres and limited local isostatic depression (Supplementary Information; 12). This makes it ideal for investigating environmental change within a Neoproterozoic panglaciation, as it provides direct evidence of subaerial environments and climatic conditions.

We made detailed sedimentary logs at ten known and new localities extending over 60 km of strike (Fig. 1; Supplementary Figure 1; see Methods). Seven sediment facies associations were identified, recording distinct depositional environments that varied in spatial extent through time (Supplementary Figure 3; Supplementary Information). These are: FA1: *Subglacial*, recording direct presence of glacier ice, FA2: *Fluvial channels*, FA3: *Dolomitic floodplain*, recording episodic flooding, evaporation and microbial communities; FA4: *Carbonate lake margin*, including evidence of wave action; FA5: *Carbonate lacustrine*, including annual rhythmites and intermittent ice-rafted debris; FA6: *Glacilacustrine*, consisting of ice-proximal grounding-line fans (FA6-G) and ice-distal rainout deposits (FA6-D); and FA7: *Periglacial,* recording cold, non-glacial conditions. Additional descriptions are provided in the Supplementary Information. The vertical and horizontal distribution of these facies associations (Fig. 1) allows the sequence of environmental changes to be reconstructed in detail.

(1) The base of the Formation is a well-marked periglacially weathered horizon with thin wind-blown sands (Supplementary Figure 4a-b). This surface records very limited sediment cycling in cold, arid conditions.

(2) At all localities, the weathering horizon is overlain by fluvial channel facies (FA2) and mudstones, marking the appearance of flowing water in the basin and implying positive air temperatures for at least part of the time (Supplementary Figure 5a).

(3) Glacilacustrine deposits (FA6-D) record flooding of the basin and delivery of sediment by ice-rafting (Supplementary Figure 4c-d). Far-travelled clasts are common, indicating transport by a large, continental ice sheet.

(4) Warm-based, active ice advanced into the basin, indicated by traction tills and glacitectonic shearing (FA1; Supplementary Figure 4e-g). (1 – 4 make up Member W1.)

(5) Ice retreat is recorded by a second periglacial weathering surface (FA7). This is overlain by fluvial channel, floodplain, lake-margin and carbonate lacustrine sediments of W2 (FA2-5; Supplementary Figure 5), recording a shifting mosaic of playa lakes and ephemeral streams. Lakes and river channels supported microbial communities. Millimetre-scale carbonate-siliciclastic rhythmites indicate seasonal cycles of photosynthesis. The environment appears to have been closely similar to that of the present-day McMurdo Dry Valleys in Antarctica, though with less extreme seasonality due to its low latitude (13).

(6) Water levels and glacier extent underwent a series of oscillations, recorded by switches between glacilacustrine diamictite (FA6-D) and fluvial, lacustrine and lake-

margin sediments (FA2-5) in W2. Sedimentation rates inferred from annual rhythmites in W2 suggest that each retreat phase may have lasted ~10^4 years.

(7) A second major ice advance marks the base of W3, with widespread deposition of subglacial tills and glacitectonism of underlying sediments. Basal tills are absent from the northernmost locality, but close proximity of glacier ice is recorded by grounding-line fans (FA6-G; Supplementary Figure 4h-i).

(8) Ice retreated while the basin remained flooded and glacigenic sediment continued to be delivered to the lake by ice rafting. Thin laminated carbonates (FA5) in W3 indicate periods of reduced glacigenic sedimentation, indicative of minor climatic fluctuations over timescales of ~10^3 years (Supplementary Figure 5g).

(9) A sharp contact with overlying laminated 'cap' carbonate (Supplementary Figure 2) records the transition to post-glacial conditions. At some localities, basal conglomerates provide evidence of subaerial exposure followed by marine transgression. The cap carbonate closely resembles basal Ediacaran carbonates elsewhere, and marks global deglaciation, eustatic sea-level rise and connection of the basin to the sea (1, 12, 14).

Environmental and atmospheric conditions during deposition of W2 and W3 can be further elucidated by isotopic data from carbonate-associated sulphate in lacustrine limestones (Fig. 2 and Supplementary Figure 6). These display negative to extremely negative $\Delta^{17}O$ values with consistent linear co-variation with $\delta^{34}S$, indicating mixing of pre-glacial sulphate and isotopically light sulphate formed in a CO_2-enriched atmosphere (15, 16). The observed values could reflect non-unique combinations of pCO_2, pO_2, O_2 residence time and other factors, but a box model (17) indicates pCO_2 was most likely ~10 to 100 mbar (1 mbar = 1000 ppmv).

94 These values are far too high to permit formation of low-latitude ice sheets in the
95 Neoproterozoic, but they are consistent with a late-stage Snowball Earth. For an ice-
96 free Neoproterozoic Earth, model studies indicate mean terrestrial temperatures in
97 the range 30-50°C for pCO_2 = 10 to 100 mbar (18). Formation of low-latitude ice
98 sheets requires much lower pCO_2, on the order of 0.1 - 1 mbar (2, 19, 20). Once
99 formed, however, ice sheets can persist despite rising CO_2 from volcanic outgassing,
100 due to high planetary albedo. This hysteresis in the relationship between pCO_2 and
101 planetary temperature is a key element of Snowball Earth theory. It implies that W2
102 and W3 were deposited relatively late in the Marinoan, after volcanic outgassing had
103 raised pCO_2 from 0.1 or 1 mbar to 10 or 100 mbar. Modeled silicate weathering and
104 volcanic outgassing rates indicate that this would require 10^6 to 10^7 years (21).
105 The consistent co-variation of $\Delta^{17}O$ and $\delta^{34}S$ in lacustrine limestones in both W2
106 and W3 suggests no detectable rise in atmospheric pCO_2, as this would alter the
107 slope of the mixing line (Fig. 2). This implies that the glacier oscillations recorded in
108 W2 and W3 occurred during a relatively short time interval ($<10^5$ years, 21) toward
109 the end of the Marinoan. In turn, this implies that the remainder of the Wilsonbreen
110 Formation (including the basal weathering horizon) represents many millions of
111 years, during which pCO_2 built up from the low values necessary for inception of low-
112 latitude glaciation to those indicated by the geochemical evidence. The weathering
113 horizon provides direct evidence of cold, arid conditions during this interval, prior to
114 the appearance of fluvial and glacilacustrine sediments in the basin.
115 The evidence for ice-sheet advance/retreat cycles at low latitudes in a CO_2-
116 enriched atmosphere motivated a series of numerical simulations to test the
117 hypothesis that these cycles were linked to Milankovitch orbital variations. We

118 employed asynchronous coupling of a 3D ice sheet model and an Atmospheric
119 General Circulation Model using the continental configuration of (22). We first ran
120 simulations with a modern orbital configuration to examine ice-sheet behaviour
121 through a large range of pCO_2 values from 0.1 to 100 mbar (23; Supplementary
122 Figures 7-10). Consistently with previous results (2, 20), at low pCO_2 (0.1 mbar),
123 global ice volume reaches 170 x 10^6 km^3 but substantial tropical land areas remain
124 ice free due to sublimation exceeding snowfall (Supplementary Figure S10a). Ice
125 volume remains relatively constant for pCO_2 = 0.1 to 20 mbar (Supplementary Figure
126 S10b), due to an increase in accumulation that compensates for higher ablation rates
127 (Supplementary Figure 13). In contrast, above 20 mbar, ice extent in the eastern
128 Tropics significantly decreases (Supplementary Figure 10c). At pCO_2 = 100 mbar,
129 most of the continental ice cover disappears except for remnants over mountain
130 ranges (Supplementary Figure 10d).
131 To test the sensitivity of the tropical ice sheets to Milankovitch forcing,
132 experiments with changing orbital parameters were initialized using the steady-state
133 ice sheets for pCO_2 = 20 mbar. Although obliquity has been invoked as a possible
134 cause of Neoproterozoic glaciations (24), this mechanism remains problematical and
135 cannot account for significant climatic oscillations at low latitudes (25, 26). We
136 therefore focused on precession as a possible driver, and used two opposite orbital
137 configurations favoring cold and warm summers, respectively, over the northern
138 tropics (CSO: cold summer orbit and WSO: warm summer orbit) (Supplementary
139 Figure 14). Switching between these configurations causes tropical ice-sheets to
140 advance/retreat over several hundred kilometers in 10 kyr (Supplementary Movie 1),
141 with strong asymmetry between hemispheres (Fig. 3). Shifting from WSO to CSO

causes ice retreat in the southern hemisphere and ice sheet expansion in the northern hemisphere (Supplementary Figure 14c-d). Significant ice volume changes occur between 30° N and S, but are less apparent in higher latitudes. This reflects higher ablation rates in the warmer low latitudes (Supplementary Figure 14e-h), and higher ice-sheet sensitivity to shifting patterns of melt. Larger greenhouse forcing at the end of the Snowball event implies increasing ice-sheet sensitivity to subtle insolation changes. Given a strong diurnal cycle (23), our simulations also predict a significant number of days above 0°C in the tropics (Supplementary Figure 15), consistent with geological evidence for ice rafting, liquid water in lakes and rivers, and photosynthetic microbial communities.

Our results show that geological evidence for glacial-interglacial cycles (5-7) is consistent with an enriched Snowball Earth theory. Termination of the Marinoan panglaciation was not a simple switch from icehouse to greenhouse states but was characterized by a climate transition during which glacial cycles could be forced by Milankovitch orbital variations. The geochemical evidence presented here implies that at least the upper 60-70% of the Wilsonbreen Formation was deposited in ~10^5 years, on the assumption that a trend in pCO_2 would be evident over longer timescales (21). Rates of CO_2 build-up, however, may have slowed in the later stages of Snowball Earth due to silicate weathering of exposed land surfaces, so it is possible that the oscillatory phase was more prolonged.

Initiation of low latitude glaciation in the Neoproterozoic requires low pCO_2 (0.1 - 1 mbar, 2, 19, 20), implying that the oscillatory phase was preceded by a prolonged colder period (~10^6 to 10^7 years) during which pCO_2 gradually increased by volcanic outgassing (21). This timescale is in agreement with recent dates indicating the

166 Marinoan lasted ~15 million years (27). The basal weathering horizon is consistent
167 with a period of low temperatures and limited hydrological cycle prior to the
168 oscillatory phase (2, 19).

169 Additional work is needed to refine the upper and lower limits of pCO_2 conducive
170 to climate and ice-sheet oscillations in Snowball Earth. Factors not included in the
171 present model, such as supraglacial dust or areas of ice-free tropical ocean (28-30),
172 can be expected to make the Earth system more sensitive to orbital forcing. While
173 many details remain to be investigated, our overall conclusions remain robust.

174 The Neoproterozoic Snowball Earth was nuanced, varied and rich. We anticipate
175 that detailed studies of the rock record in other parts of the world, in conjunction
176 with numerical modeling studies, will continue to yield insight into the temporal and
177 regional diversity of this pivotal period in Earth history.

178

179

180 **Methods**

181

182 **Sedimentology.** Lithofacies were classified based on grain size, internal sedimentary
183 structures and deformation structures, and bounding surfaces. Detailed stratigraphic
184 logs were made in the field, supplemented by drawings and photographs of key
185 features. Samples were taken for polishing and thin sectioning, to allow detailed
186 examination of microstructures in the laboratory. In addition, data were collected on
187 clast lithology, shape, surface features and fabric. Diamictites of the Wilsonbreen
188 Formation are commonly very friable, allowing included clasts to be removed intact
189 from the surrounding matrix, allowing measurement of both clast morphology and

orientation, using methods developed for unlithified sediments. Clast morphology (shape, roundness and surface texture) was measured for samples of 50 clasts to determine transport pathways. Clast fabric analysis was performed by measuring a-axis orientations of samples of 50 clasts with a compass-clinometer, and data were summarized using the eigenvalue or orientation tensor method. Orientated samples for measurement of Anisotropy of Magnetic Susceptibility (AMS) were collected using a combination of field-drilling and block sampling. AMS was measured using an AGICO KLY-3 Kappabridge operating at 875 Hz with a 300 A/m applied field at the University of Birmingham and an AGICO MFK-1A Kappabridge operating at 976 Hz with a 200 A/m applied field at New Mexico Highlands University.

Geochemistry. Laboratory procedures for extracting, purifying, and measuring the triple oxygen ($\delta^{18}O$ and $\Delta^{17}O$) and sulfur ($\delta^{34}S$) isotope composition of CAS in bulk carbonates are detailed in ref 16. Briefly, fresh carbonate-bearing rock chips were crushed into fine grains and powders using mortar and pestle. Rinsing the fines with 18 MΩ water revealed little water-leachable sulphate in all the Wilsonbreen carbonates. Subsequently, ca. 10 to 30 g carbonates were slowly digested in 1-3 M HCl solutions. The solution was then centrifuged, filtered through a 0.2 μm filter, and acidified before saturated $BaCl_2$ droplets were added. $BaSO_4$ precipitates were collected after >12 hours and purified using the DDARP method (see Supporting Information). The purified $BaSO_4$ was then analyzed for three different isotope parameters: 1) $\Delta^{17}O$, by converting to O_2 using a CO_2-laser fluorination method; 2) $\delta^{18}O$, by converting to CO through a Thermal Conversion Elemental Analyzer (TCEA) at 1450 °C; and 3) $\delta^{34}S$, by converting to SO_2 by combustion in tin capsules in the

presence of V_2O_5 through an Elementar Pyrocube elemental analyzer at 1050 °C. The $\Delta^{17}O$ was run in dual-inlet mode while the $\delta^{18}O$ and $\delta^{34}S$ in continuous-flow mode. Both the $\Delta^{17}O$ and $\delta^{18}O$ were run on a MAT 253 at Louisiana State University whilst the $\delta^{34}S$ was determined on an Isoprime 100 continuous flow mass spectrometer at the University of Lancaster, UK. The $\Delta^{17}O$ was calculated as $\Delta^{17}O \equiv \delta'^{17}O - 0.52 \times \delta'^{18}O$ in which $\delta' \equiv 1000\ln(R_{sample}/R_{standard})$ and R is the molar ratio of $^{18}O/^{16}O$ or $^{17}O/^{16}O$. All δ values are in VSMOW and VCDT for sulphate oxygen and sulfur respectively. The analytical standard deviation (1σ) for replicate analysis associated with the $\Delta^{17}O$, $\delta^{18}O$, and $\delta^{34}S$ are ±0.05‰, ±0.5‰, and ±0.2‰, respectively. Since the CAS is heterogeneous in hand-specimen, the standard deviation is for laboratory procedures. $\delta^{34}S$ values were corrected against VCDT using within run analyses of international standard NBS-127 (assuming $\delta^{34}S$ values of +21.1 ‰). Within-run standard replication (1 SD) was <0.3 ‰. All geochemical data are included in Supplementary Table 1.

Numerical modeling. Model runs were conducted with a coupled atmospheric general circulation model (LMDz) and ice-sheet model (GRISLI: GRenoble Ice Shelf and Land Ice model). LMDz (spatial resolution 4° in latitude x 5° in longitude with 38 vertical levels) was run with prescribed continental ice to climatic equilibrium. GRISLI has a 40km grid size and is driven with downscaled climatic fields of surface air temperature, precipitation and evaporation. To capture ice sheet – climate feedbacks, LMDz is rerun using the new ice sheet distribution and topography. This procedure was repeated each 10 kyr to investigate orbital forcing.

Surface mass balance (accumulation minus sublimation and melting) was computed from monthly mean temperature, precipitation and evaporation rate. Melt rate is calculated using the Positive Degree Day method.

No sea ice dynamics treatment is specified, the sea ice cover is prescribed and a thickness of 10 meters is imposed. Ice albedo is fixed at 0.6, while snow albedo varies from 0.9 from 0.55 as a function of the zenith, and ageing process. Land ice/snow free surface has the characteristic of a bare soil (rocky regolith) with an albedo of 0.3.

Code availability. Code for the GCM LMDz can be accessed at: http://lmdz.lmd.jussieu.fr. Code for the ISM GRISLI (GRenoble Ice Shelf and Land Ice model) is not available.

Additional details of the methods and modeling procedures are provided in the Supplementary Information in the online version of the paper.

References

(1) Hoffman, P.F. and Schrag, D.P. The Snowball Earth hypothesis: testing the limits of global change. *Terra Nova* **14**, 129-155 (2002).

(2) Donnadieu, Y., Goddéris, Y. and Le Hir, G. Neoproterozoic atmospheres and glaciation. In: *Treatise on Geochemistry*, Second Edition Vol. 6, 217-229 (2014).

(3) Hoffman, P.F. Strange bedfellows: glacial diamictite and cap carbonate from the Marinoan (635Ma) glaciation in Namibia. *Sedimentology* **58**, 57-119 (2011).

(4) Allen, P.A. and Etienne, J.L. Sedimentary challenge to Snowball Earth. *Nat Geosci* **1**, 817-825 (2008).

(5) Rieu, R., Allen, P.A., Plötze, M. and Pettke, T. Climatic cycles during a Neoproterozoic "snowball' glacial epoch. *Geology* **35**, 299-302 (2007).

(6) Le Heron, D.P., Busfield, M.E., and Kamona, F. An interglacial on snowball Earth? Dynamic ice behaviour revealed in the Chuos Formation, Namibia. *Sedimentology* **60***,* 411-427 (2013).

(7) Fairchild, I.J. and Hambrey, M.J. Vendian basin evolution in East Greenland and NE Svalbard. *Precambrian Res* **73**, 217–233 (1995).

(8) Halverson, G.P. A Neoproterozoic Chronology IN: Xiao, S. & Kaufman, A.J. (Eds.) *Neoproterozoic Geobiology and Paleobiology*, 231-271 (Springer, New York, 2006).

(9) Li, X.-X., Evans, D.A. and Halverson, G.P. Neoproterozoic glaciations in a revised global palaeogeography from the breakup of Rodinia to the assembly of Gondwanaland. *Sediment Geol* **294**, 219-232 (2013).

(10) Petronis, M S, Stevenson, C, Fleming, E J, Fairchild, I J, Hambrey, M, Benn, D I., 2013, Paleomagnetic Data from the Neoproterozoic Wilsonbreen Formation, Ny Friesland, Svalbard, Norway and Preliminary Data from the Storeelv Formation, Ella Ø, Kong Oscar Fjord, East Greenland, American Geophysical Union, Fall Meeting 2013, abstract #GP41A-1107.

(11) Harland, W.B. *The Geology of Svalbard*. Geol. Soc. London Mem., 17 (Geological Society, London, 1997).

(12) Creveling, J.R. and Mitrovica, J.X. The sea-level fingerprint of a Snowball Earth deglaciation. *Earth Planet Sc Lett* **399**, 74–85 (2014).

(13) Lyons, W.B. et al. The McMurdo Dry Valleys long-term ecological research program: new understanding of the biogeochemistry of the Dry Valley lakes: a review. *Polar Geography* **25**, 202-217 (2001).

(14) Hoffman, P. et al. Are basal Ediacaran (635 Ma) basal 'cap dolostones' diachronous? *Earth Planet Sc Lett* **258**, 114-131 (2007).

(15) Fairchild, I.J., Hambrey, M.J., Spiro, B. and Jefferson, T.H. Late Proterozoic glacial carbonates in northeast Spitsbergen: new insights into the carbonate-tillite association. *Geol Mag* **126**, 469-490 (1989).

(16) Bao, H., Fairchild, I.J, Wynn, P.M. and Spötl, C. Stretching the envelope of past surface environments: Neoproterozoic glacial lakes from Svalbard. *Science* **323**,119-122 (2009).

(17) Cao, X. and Bao, H. Dynamic model constraints on oxygen-17 depletion in atmospheric O_2 after a Snowball Earth. P Natl Acad Sci USA **110**, 14546–14550 (2013).

(18) Le Hir, G. et al. The snowball Earth aftermath: Exploring the limits of continental weathering processes. *Earth Planet Sc Lett* **277**, 453–463 (2009).

(19) Pierrehumbert, R., Abbot, D.S., Voigt, A. and Koll, D. Climate of the Neoproterozoic. *Ann Rev Earth Planet Sci* **39**, 417-460 (2011).

(20) Pollard, D. and Kasting, J.F. Climate-ice simulations of Neoproterozoic glaciation before and after collapse to Snowball Earth. In: G.S. Jenkins, M.A.S. McMenamin, C.P. McKay and L. Sohl (eds.) *The Extreme Proterozoic: Geology, Geochemistry, and Climate.* Geophys. Monogr. Ser. 146 (AGU, Washington, D.C. 2004).

(21) Le Hir, G., Ramstein, G., Donnadiieu, Y. and Goddéris, Y. Scenario for the evolution of atmospheric pCO_2 during a snowball Earth. *Geology* **36**, 47–50 (2008).

(22) Hoffman, P.F., Li, Z.X., A palaeogeographic context for Neoproterozoic glaciation. *Palaeogeogr Palaeocl* **277**, 158–172 (2009).

(23) Pierrehumbert, R.T. Climate dynamics of a hard Snowball Earth. *J Geophys Res* **110**, DOI: 10.1029/2004JD005162 (2005).

(24) Spiegl, T. C., Paeth, H. and Frimmel, H.E., Evaluating key parameters for the initiation of a Neoproterozoic Snowball Earth with a single Earth System Model of intermediate complexity. *Earth Planet Sc Lett* **415**, 100-110 (2015).

(25) Donnadieu, Y., Ramstein, G., Fluteau, F., Besse, J. and Meert, J. Is high obliquity a plausible cause for Neoproterozoic glaciations? *Geophys Res Lett* **29**, DOI: 10.1029/2002GL015902 (2002).

(26) Paillard, D. Quaternary glaciations: from observations to theories. *Quaternary Sci Rev* **107**, 11-24 (2015).

(27) Rooney, A.D. et al. A Cryogenican chronology: Two long-lasting synchronous Neoproterozoic glaciations. Geology 43, 459-462 (2015).

(28) Abbot, D.S. and Pierrehumbert, R.T. Mudball: surface dust and Snowball Earth deglaciation. J Geophys Res **115,** DOI: 10.1029/2009JD012007 (2010).

(29) Abbot, D.S., Voigt, S. and Koll, D. The Jormungand global climate state and implications for Neoproterozoic glaciations. *J Geophys Res-Atmos* 116, DOI: 10.1029/2011JD015927 (2011).

(30) Rose, B. E. J. Stable "Waterbelt" climates controlled by tropical ocean heat transport: A nonlinear coupled climate mechanism of relevance to Snowball Earth. *J Geophys Res-Atmos* **120**, doi:10.1002/2014JD022659 (2015).

Correspondence and requests for materials should be addressed to Doug Benn (doug.benn@unis.no).

Acknowledgements

This work was supported by the NERC-funded project GR3/ NE/H004963/1 Glacial Activity in Neoproterozoic Svalbard (GAINS). Logistical support was provided by the University Centre in Svalbard. This work was granted access to the HPC resources of CCRT under allocation 2014-017013 made by GENCI (Grand Equipement National de Calcul Intensif). We also thank Didier Paillard and Paul Hoffman for stimulating discussions and valuable insights.

Author contributions

Field data were collected and analyzed by IJF, DIB, EJF, MJH, EAMcM, MSP, PMW and CTES. Geochemical analyses were conducted by HB and PMW. Model experiments were designed and conducted by GLeH, YD, CD and GR. The manuscript and figures were drafted by DIB, IJF and GLeH, with contributions from the other authors.

Competing financial interests

The authors declare no competing financial interests.

Figures:

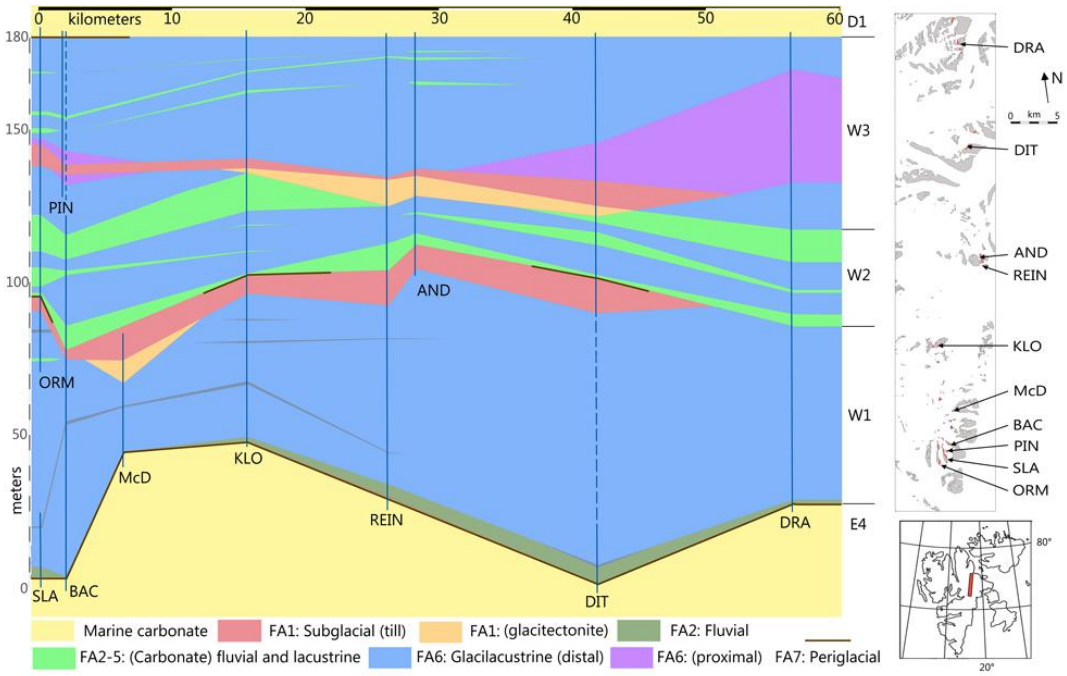

Figure 1: Sedimentary architecture and palaeoenvironments of the Wilsonbreen Formation. Regional correlation of facies associations and members W1, W2 and W3 across NE Svalbard. From north to south, study locations are: DRA: Dracoisen; DIT: Ditlovtoppen; AND: East Andromedafjellet; REIN: Reinsryggen (informal name); KLO: Klofjellet; McD: MacDonaldryggen; BAC: Backlundtoppen - Kvitfjellet ridge; PIN: Pinnsvinryggen (informal name); SLA: Slangen and ORM: Ormen.

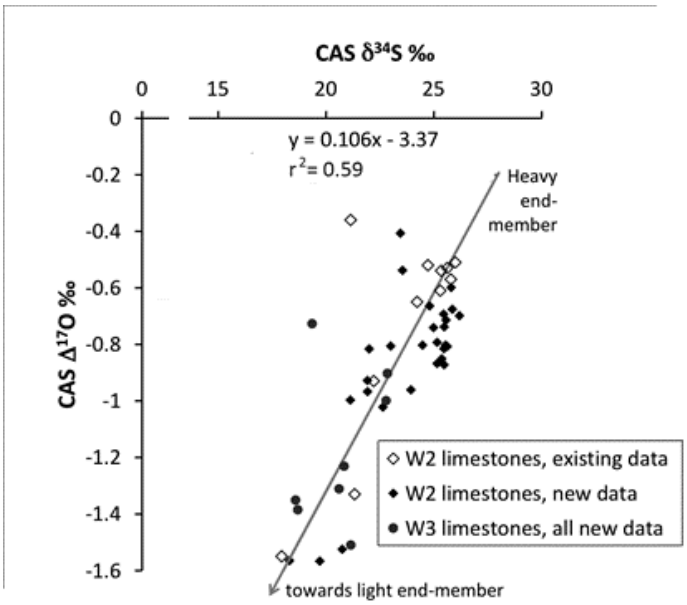

Figure 2: Co-variation of $\Delta^{17}O$ and $\delta^{34}S$ from carbonate-associated sulphate in W2 and W3. Existing data (ref. 16) and new data define a mixing line between pre-glacial sulphate (top) and an isotopically light sulphate formed by oxidation of pyrite including incorporation of a light-$\Delta^{17}O$ signature from a CO_2-enriched atmosphere. Data from W2 and W3 lie on closely similar trend lines, indicating no detectable change in pCO_2 between deposition of the two members.

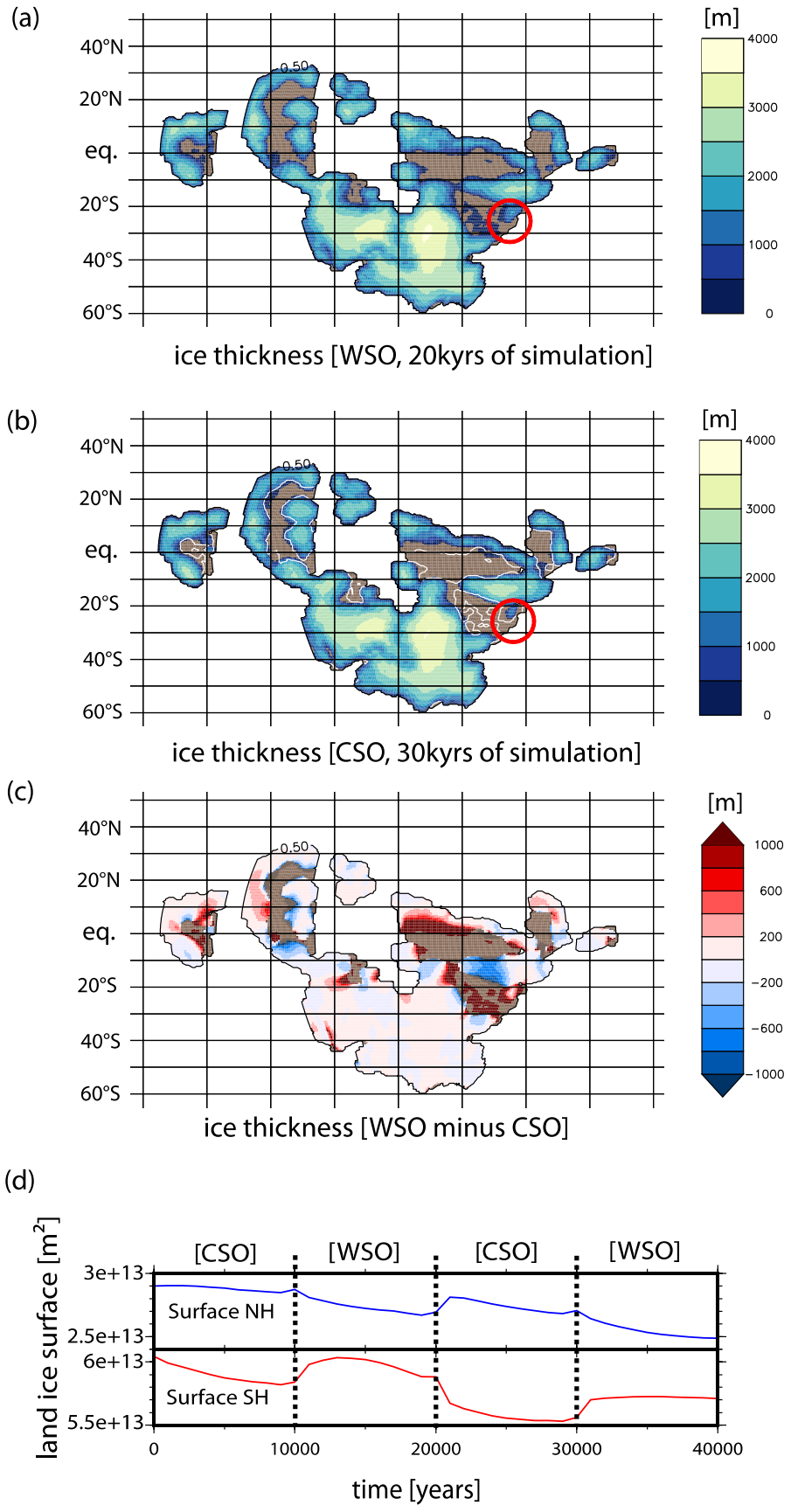

Figure 3: Modelled ice sheet oscillations in response to orbital forcing. (a), (b) Land

ice thickness obtained with 20 mbar of carbon dioxide in response to changes of orbital forcing (WSO and CSO, warm/cold summer orbit for the northern hemisphere) over the course of two precession cycles (40 ky of simulation). Continental areas without ice are light brown, the white line is used to represent the old ice-sheet extension (WSO case). The Svalbard area is indicated by a red circle. (c) ice thickness variation in 10 ky (WSO case after 20 ky minus CSO case after 30 ky of simulation) (d) area covered by ice (m^2) in each hemisphere through time ([WSO] and [CSO] indicate which orbital configuration is used).